

Artificial Intelligence-Assisted Loop Mediated Isothermal Amplification (ai-LAMP) for Rapid and Reliable Detection of SARS-CoV-2

Mohammed A Rohaim^a, Emily Clayton^a, Irem Sahin^a, Julianne Vilela^a, Manar Khalifa^a, Mohammad Al-Natour^a, Mahmoud Bayoumi^a, Aurore Poirier^b, Manoharanehru Branavan^c, Mukunthan Tharmakulasingam^f, Nouman S Chaudhry^f, Ravinder Sodi^d, Amy Brown^e, Peter Burkhardt^e, Wendy Hacking^e, Judy Botham^e, Joe Boyce^e, Hayley Wilkinson^e, Craig Williams^e, Michelle Bates^a, Roberto La Ragione^b, Wamadeva Balachandran^c, Anil Fernando^f, Muhammad Munir^{a*}

^aDivision of Biomedical and Life Sciences, The Lancaster University, UK; ^bDepartment of Pathology and Infectious Diseases, School of Veterinary Medicine, University of Surrey, Guildford, UK; ^cCollege of Engineering, Design and Physical Sciences, Brunel University London, Kingston Lane, Uxbridge, UK; ^dDepartment of Biochemistry, Poole & Bournemouth Hospitals NHS Trust, Longfleet Road, Poole, UK BH15 2JB; ^eThe Royal Lancaster Infirmary, University Hospitals of Morecambe Bay NHS, Foundation Trust, UK; ^fCentre for Vision, Speech and Signal Processing, University of Surrey, UK.

*Correspondence: muhammad.munir@lancaster.ac.uk

Abstract

Until vaccines and effective therapeutics become available, the practical way to transit safely out of the current lockdown may include the implementation of an effective testing, tracing and tracking system. However, this requires a reliable and clinically validated diagnostic platform for the sensitive and specific identification of SARS-CoV-2. Here, we report on the development of a *de novo*, high-resolution and comparative genomics guided reverse-transcribed loop-mediated isothermal amplification (LAMP) assay. To further enhance the assay performance and to remove any subjectivity associated with operator interpretation of result, we engineered a novel hand-held smart diagnostic device. The robust diagnostic device was further furnished with automated image acquisition and processing algorithms, and the collated data was processed through artificial intelligence (AI) pipelines to further reduce the assay run time and the subjectivity of the colorimetric LAMP detection. This advanced AI algorithm-implemented LAMP (ai-LAMP) assay, targeting the RNA-dependent RNA polymerase gene, showed high analytical sensitivity and specificity for SARS-CoV-2. A total of ~200 coronavirus disease (CoVID-19)-suspected patient samples were tested using the platform and it was shown to be reliable, highly specific and significantly more sensitive than the current gold standard qRT-PCR. The system could provide an efficient and cost-effective platform to detect SARS-CoV-2 in resource-limited laboratories.

Key words: SARS-CoV-2, diagnosis, LAMP, point of care, artificial intelligence

NOTE: This preprint reports new research that has not been certified by peer review and should not be used to guide clinical practice.

49 Introduction

50

51 A cluster of new pneumonia cases was reported to the World Health Organization
52 (WHO) in late 2019 from Wuhan, Hubei Province of China. The causative agent was
53 named as severe acute respiratory syndrome coronavirus 2 (SARS-CoV-2) and led to
54 a global pandemic [1–3]. While the major impact of SARS-CoV-2 was attributed to frail
55 and elderly people with co-morbidities, coronavirus disease 2019 (CoVID-19) was
56 mainly spread by asymptomatic or mildly symptomatic patients [2]. Due to their high
57 mutation rates and recombination events, coronaviruses can infect a range of animal
58 species including humans, avian, rodents, carnivores, chiropters and other mammals
59 [4]. Before the emergence of SARS-CoV-2, a total of six different coronaviruses were
60 reported to infect humans, including HCoV-229E, HCoV-OC43, HCoV-NL63, HCoV-
61 HKU1, MERS and SARS-CoV-1 (also known as classical SARS). The SARS-CoV-2
62 belongs to the β -coronavirus of the group 2B within the family of *Coronaviridae* [3].

63

64 The SARS-CoV-2 shares a high level of genetic similarity (up to 96%) with
65 coronaviruses originating from bats [3]. The genome of β -coronavirus encodes for the
66 replicase complex (ORF1ab), spike (S), envelope (E), membrane (M) and
67 nucleoprotein (N) genes in addition to the several non-structural and accessory
68 proteins in the order from 5'-untranslated to 3'-untranslated regions [3]. Owing to the
69 nature of viral genetics, the N gene is the most transcribed and highly conserved gene
70 within the *Coronaviridae* family and has been a major target for both antigen and
71 antibodies diagnostics. Across the genome, the RNA-dependent RNA polymerase
72 (RdRP), encoded by the ORF1b gene segment, presents a high level of intra-group
73 conservation and therefore is an ideal target for a diagnostic application [5, 6].

74

75 As evident by previous pandemics caused by coronaviruses, a highly specific,
76 sensitive and easily deployable diagnostic is critical for the identification, tracing,
77 rationalizing control measures and documentation of asymptomatic carriers and
78 clinically evident patients [7- 9]. Additionally, due to the unavailability of the registered
79 vaccines or effective therapeutics, rapid and reliable diagnostics are of paramount
80 importance to curtail SARS-CoV-2 infection. Because of shortcomings associated with
81 the virus isolation (time consuming and required containment) and cross-reactivities
82 of antigen and antibodies assay, several real-time reverse transcription-polymerase
83 chain reactions (qRT-PCR) and reverse-transcription loop mediated isothermal
84 amplification (RT-LAMP) assays have been developed, validated and commercialized
85 as useful laboratory diagnostics for the detection of SARS-CoV-2 [10]. However, the
86 majority of these assays are time-consuming and require laboratory-intense
87 instrumentation. Furthermore, they are unable to meet the current unprecedented
88 rapid growth and demand for testing a large proportion of the population, identification
89 of asymptomatic carriers and contact tracing.

90

91 Though qRT-PCR remains the gold standard for the diagnosis of SARS-CoV-2, RT-
92 LAMP assays have been demonstrated to produce diagnostic results with increased
93 sensitivity and specificity [11]. Furthermore, its ability to tolerate PCR inhibitors
94 eliminates the need for laborious RNA extraction and purification methodologies [12,
95 13]. Several platforms capable of performing LAMP assays in the field have previously
96 been documented [14]. However, most platforms have employed fluorescence
97 detection with integrated optical units or a smart phone dock to achieve detection [15,
98 16]. Similarly, for colorimetric LAMP assays, smart phone cameras or user

99 interpretation of the colour changes were used to achieve detection [17, 18]. The fully
100 integrated real-time fluorescence-based platforms are expensive, and the
101 smartphone-based platforms are only designed for specific smartphone models.
102 Therefore, to fulfil the need for a standalone colorimetric isothermal nucleic acid
103 amplification platform [19], we have developed an ultra-low-cost molecular diagnostic
104 device with an integrated single-board computer, imaging camera, artificial
105 intelligence-based image processing algorithm and mobile app.

106
107 In this study, we developed a high-resolution comparative genomics analysis-guided
108 novel RT-LAMP assay for the specific and sensitive detection of SARS-CoV-2 in
109 comparison to WHO recommended qRT-PCR assays. In order to provide a simple
110 “sample-to-answer workflow”, an ultra-low-cost and user-friendly diagnostic platform
111 was engineered and was further supplemented with a module for automated image
112 acquisition and processing. Artificial intelligence-guided assessment of the LAMP
113 assay provided faster detection of colour changes in the LAMP reaction to further
114 enhance the assay performance and to reduce the human error in results
115 interpretation. Finally, the assay was validated on clinical samples from CoVID-19
116 suspected patients to demonstrate the real-life applicability.

117 118 **1. Material and Methods**

119 120 **1.1. Ethics statement**

121 This study was conducted in accordance with the University Human ethics guidelines
122 and received a favourable review from the Faculty of Health and Medicine Research
123 Ethics Committee (FHMREC) of Lancaster University - reference number
124 FHMREC19112. The study was exempt from requiring specific patient consent, as it
125 only involved the use of extracted RNA and existing collections of data or records that
126 contained non-identifiable data about human patients.

127 128 **1.2. Cells and viruses**

129 Vero cells and MDCK cells were grown in Dulbecco’s modified Eagle’s medium
130 (DMEM) (Gibco, Carlsbad, CA) supplemented with 10% inactivated foetal bovine
131 serum (FBS) (Gibco), 2 mM L-glutamine (Gibco) and 100U/mL penicillin/streptomycin
132 (Gibco) at 37°C in 5% CO₂. Influenza A virus (A/chicken/Pakistan/UDL-
133 01/2008(H9N2), Newcastle disease virus strain LaSota and Infectious bronchitis virus
134 strain H120, Vesicular stomatitis virus (VSV) and Sendai virus (SeV) were propagated
135 and used to determine the specificity of the LAMP. All viruses except influenza were
136 titrated on Vero and MDCK cells, respectively by the standard plaque assay.

137 138 **1.3. *In silico* nucleotide sequence comparisons and primer design**

139 To design specific LAMP primer sets for the detection of SARS-CoV-2, all available
140 complete genome sequences were downloaded from GISAID Initiative
141 (<https://www.gisaid.org/>), aligned and the conserved part was selected and used as
142 the template of LAMP primer design. To find out an efficient primer set, three sets of
143 specific LAMP primers were hand-picked and validated using PrimerExplorer V5
144 software (<http://primerexplorer.jp/elamp4.0.0/index.html>). Primers were validated
145 using BLAST software (<http://www.ncbi.nlm.gov/BLAST>) to ensure their specificity.

146 147 **1.4. Cloning and *in vitro* transcription of RdRP target gene**

148 The coding sequence of SARS-CoV-2 RdRp gene was chemically synthesized and
149 cloned into *pVAX1* plasmid (Invitrogen, Carlsbad, USA) between *KpnI* and *NotI*
150 restriction sites. The plasmid was propagated in DH5 α cells and purified using
151 MiniPrep Qiagen Kits. The linearized plasmid with *pVAX1*-RdRP was used for *in vitro*
152 transcription using T7 RiboMAX™ Express Large-Scale RNA Production System
153 (Promega, USA). The copy number of *in vitro* transcribed RNA was calculated from
154 RNA concentration measured with NanoDrop™ 2000c Spectrophotometers (Thermo,
155 USA) in triplicate. RNA products were then purified using the RNeasy MinElute
156 Cleanup Kit (Qiagen, Valencia, CA, USA). A standard curve was generated using
157 dilutions of the standard *in vitro* transcribed RNAs using *SuperScript III Platinum One-*
158 *Step qRT-PCR Kit* as per the manufacturer's protocol (Invitrogen, Carlsbad, USA)
159 using CFX384 Touch Real-Time PCR Detection System is (Applied Biosystems,
160 USA).

161

162 **1.5. Clinical sample processing and spiking with miR-cel-miR-39-3p RNA**

163 A total of 199 nasopharyngeal swabs were individually collected from CoVID-19
164 suspected patients, through routine NHS collection procedure. These samples were
165 stored and transported in the virus transport media (VTM) to the diagnostic laboratory
166 at Lancaster University, UK. All samples were individually spiked with 50 pmol/L of
167 synthesized *Caenorhabditis elegans* miR-cel-miR-39-3p (Applied Biosystems/Ther-
168 mo-Fisher Scientific, UK). The miR-cel-miR-39-3p RNA lacked any sequence
169 homology to human or viral gene and thus present an ideal RNA extraction control.
170 Total RNA including miRNAs was extracted using 140 μ L of the spiked-VTM by the
171 commercial QIAampViral RNA Mini kit (QIAGEN, Valencia, California). The miR-cel-
172 miR-39-3p RNA was used to serve as an internal control to monitor extraction
173 efficiency and used for data normalisation. The final RNA yield and purity were
174 determined by the A260/A280 ratio measured by a NanoDrop ND-1000
175 spectrophotometer (NanoDrop Technologies/Thermo-Fisher Scientific, UK) with a
176 ratio of 1.80 to 2.00 indicative of good RNA purity. The isolated RNA was stored at
177 -80°C for further use.

178

179 **1.6. Real-time fluorescent-based quantitative PCR.**

180 Suspected samples with SARS-CoV-2 were tested for positivity by qRT-PCR. Briefly,
181 RNA was extracted from Viral Transport Media using the QIAamp Viral RNA Mini kit
182 (QIAGEN, Valencia, California) following the manufacturer instructions. The qRT-PCR
183 was conducted using the *SuperScript III Platinum One-Step qRT-PCR Kit* as per the
184 manufacturer's protocol (Invitrogen Carlsbad, USA) in the CFX384 Touch Real-Time
185 PCR Detection System (Biorad, USA), according to the cycling protocol. The reaction
186 was performed using the specific primer set RdRpF; RdRpR and FAM-labelled probe
187 or NP-F; NP-R and ROX labelled probes designed to detect SARS-CoV2. The 25- μ L
188 PCR reaction consists of 12.5 μ L 2X Reaction Mix, 0.2 μ M of each primer, and 0.1 μ M
189 probe, 0.5 μ L of SuperScript® III RT/Platinum® Taq Mix, 5 μ L of RNA sample and
190 nuclear free water. The cycling program was performed in the CFX384 Touch Real-
191 Time PCR Detection System is (Applied Biosystems, USA), according to the cycling
192 protocol. The amount of viral RNA in each sample was estimated by comparing the
193 cycle threshold values (Ct) to the standard curve made by serial 10-fold serial dilutions
194 of previously titrated *in vitro* transcribed RdRP gene.

195

196 **1.7. ai-LAMP assay performance**

197 All experiments for LAMP were run in triplicate. The LAMP reactions were performed
198 using WarmStart™ Colorimetric LAMP 2X Master Mix (New England Biolabs). A 10X
199 primer mix (FIP, 16 µM; BIP, 16 µM; F3, 2 µM; B3, 2 µM; LF, 4 µM; LB, 4 µM) was
200 prepared. A 25 µl reaction mixture (12.5 µl 2X MasterMix; 2.5 µl 10X primer mix; 2.5
201 µl RNA and 7.5 µl DNase & RNase-free molecular grade water) was mixed
202 homogeneously and centrifuged. The LAMP was performed in a thermocycler
203 (MJResearch) at 65°C for 30 min or in the engineered device (**Figure 4A**). Colour
204 change was observed directly by the naked eye or through image processing, and
205 agarose gel electrophoresis was performed to confirm the results. The completion of
206 amplification was indicated by the colour in the tube, wherein yellow was considered
207 positive and pink was regarded as negative. The amplicon was confirmed by 2%
208 agarose gel electrophoresis.

209

210 **1.8. Artificial intelligence based test-tube colour detection**

211 A loop-mediated isothermal amplification (LAMP) assay based COVID-19 test device
212 was proposed to obtain the COVID-19 test results in 30 minutes based on colour
213 changes. Artificial intelligence (AI) based colour detection was proposed to identify
214 colour changes considering different lighting issues and to reduce the test running
215 time less than 30 minutes. Images were acquired from the COVID-19 test kit which
216 carried 8 test-tubes including NTC (negative test control) and PTC (positive test
217 control) for every 20 seconds during the test operation. Each image was cropped into
218 separate tubes using template matching approach and labelled manually based on
219 their colour.

220

221 **1.9. Analytical specificity and analytical sensitivity of LAMP**

222 The designed RdRp primer sets for LAMP to detect SARS-CoV-2 were validated for
223 their specificity by testing the cross-reactivity with other viruses, including influenza A
224 virus, Vesicular stomatitis virus (VSV), Sendai virus (SeD), infectious bronchitis virus
225 (IBV) and Newcastle disease virus (NDV). Likewise, the developed LAMP assay was
226 evaluated to test the primers set sensitivity in a serially diluted standard RNA template
227 prepared by tenfold serial dilutions. The amplification patterns were observed for each
228 dilution to determine the lowest amount of absolute RNA template required for
229 detectable amplification. The degree of colour intensity of the amplified product as well
230 as the observed electrophoretic pattern during gel electrophoresis was used for the
231 analysis of LAMP amplification.

232

233 **1.10. Quantitative real time PCR for miR-cel-miR-39-3p RNA**

234 In order to determine the RNA extraction efficiency, the extracted RNA was reverse
235 transcribed using a commercially available kit (Applied Biosystems/Thermo-Fisher
236 Scientific, UK) using miR-specific stem-loop primers as per manufacturer instructions.
237 A total of 5 µL of the sample was added to a 96-well plate together with 10 µL reaction
238 mixture (MasterMix™) containing along with Multiscribe™ reverse transcriptase (50
239 U/µL), and 0.19 µL RNAase inhibitor (20 U/µL). The RT reaction was performed at 16
240 °C for 30 min, followed by 42 °C for 30 min, and 85 °C for 5 min and was finally kept
241 at 4 °C. A NTC was considered in every individually run reaction to identify any
242 unspecific amplification. The RT products were quantified immediately by qPCR using
243 TaqMan™ MicroRNA assays (Applied Biosystems/Thermo-Fisher Scientific, UK) in
244 a 96 well plate using the 7900HT Fast Real-Time PCR System (Applied Biosystems,
245 UK) as we described before [37]. The quantification cycle (Cq) was determined with

246 instrument default threshold settings (10 SDs above the mean fluorescence of the
247 baseline cycle).

248

249 **1.11. Statistical analysis**

250 GraphPad Prism Software version 6.01 for Mac (GraphPad Software, La Jolla,
251 California, USA) was used for graphs generation. The LAMP detection sensitivity and
252 specificity were calculated using the chi-squared test. TPR (true positive rate), TNR
253 (true negative rate), FPR (false positive rate), FNR (false negative rate) were
254 calculated according to the following equations: $TPR = TP / (TP + FN)$.
255 $TNR = TN / (FP + TN)$. $FNR = FN / (TP + FN)$. $FPR = FP / (FP + TN)$. TP: total number of true
256 positives. TN: total number of true negatives. FN: total number of false negatives.
257 total number of false negatives.

258

259 **2. Results**

260

261 **2.1. High resolution conversation analysis of SARS-CoV-2 to guide promising 262 oligos design**

263 It is imperative to critically assess the evolving nature of viruses in identifying
264 conserved gene signatures and guiding the selection of the most appropriate primers.
265 In order to identify important genomic loci, we downloaded and aligned all the available
266 full-length genomes with high coverage sequences ($n=22858$) of SARS-CoV-2 by
267 Multiple Alignment using Fast Fourier Transform (MAFFT) [20]. We then compiled *in*
268 *house* R-code (available on request) to determine the single nucleotide-based genetic
269 conservation across the length of ~30kb genome. The analysis of the aligned dataset
270 of all genomes in the RStudio generated a total of 18GB high-resolution nucleotide-
271 by-nucleotide score from 0.0 to 1.0 (1.0 being the highly conserved and 0.0 being the
272 highly divergent). Plotting the assessed genetic divergence, at a cut point of 90%
273 similarity along with the genome of the SARS-CoV-2, identified sharp divergence at
274 multiple loci (**Figure 1A**). However, most of the genomes maintained high
275 conservation. The divergence at the 5' and 3' ends was primarily due to length
276 heterogeneity, which may be partly as a result of sequencing artifact or potentially
277 coronaviruses ragged termini (**Figure 1B**). Owing to high divergence, a stretch of
278 sequence (~400 nucleotides, numbering corresponds to the complete genome of
279 strain SARS-CoV-2/human/USA/VA-DCLS-0285/2020 strain, GenBank Accession
280 Number: MT558705.1) spanning the start of the ORF1b, which encode for viral RNA-
281 dependent RNA polymerase (RdRP), was targeted to design oligos for the LAMP
282 assay. Additionally, this specific target genomic locus was adjacent to oligos
283 recommended by the World Health Organization (WHO) and Public Health England
284 (PHE) for real-time RT-PCR-based routine identification of CoVID-19 patients, further
285 allowing direct and comparable evaluation of real-time RT-PCR with *de novo*
286 developed LAMP assay (**Figure 1C**).

287

288 The conserved region of the RdRP gene with the lowest mutation frequencies was
289 used as a template to manually design three sets of basic LAMP primers and selected
290 with PrimerExplorer V5 for appropriate primer lengths, loop selection and melting
291 temperature optimization (**Figure 1C**). In order to preclude the non-specific
292 amplification of common coronaviruses, efforts were made to design primers in the
293 regions where there is a high level of divergence among more than 3 of the 6 total
294 primers in a specific set. Amongst the most suitable targets, the primers with high
295 scores were aligned with MERS-CoV, hCoV-229E, hCoV-OC43, hCoV-NL63, hCoV-

296 HKU1 and SARS-CoV-1 (**Figure 1D**). These selected primers were used for further
297 validation and screening.

298

299 **2.2. Determination of limit of detection using biochemically synthesis RNA**

300 In order to assess the robustness of the primers, we used a fully identical *in vitro*
301 transcribed target RNA unanimously spanning the length of the RdRP-gene based
302 LAMP and qRT-PCR target regions. The pre-determined copy numbers of the
303 biochemically synthesised RNA were 10-fold serially diluted from 10^7 copies to 0
304 copies of the target gene per reaction. To determine the analytical sensitivity of the
305 assays, we first evaluated their limits of detection (LoD) for both qRT-PCR and LAMP
306 assays. The LoD of the qRT-PCR was 10 copies as evident from the relative
307 fluorescence units (**Figure 2A**) and electrophoreses of the amplified products (**Figure**
308 **2B**). The standard curve generated by the RdRP-based qRT-PCR was linear and
309 generated a coefficient of correlation (R^2) = 0.9481 and a slope of -2.6509 (**Figure**
310 **2C**). Melting curve analysis revealed the specificity of primers for the target gene
311 sequence, as all the amplified products showed a uniform melting temperature (T_m)
312 of $\sim 75.10^\circ\text{C}$ and specific amplification patterns (**Figure 2B** and data not shown).
313 Compared to the qRT-PCR assay, the LoD for the LAMP which targeted the same
314 RdRP gene was 1 log unit higher (10^2 copies/reaction) (**Figure 2D**, upper panel) as
315 assessed by visual observation of the LAMP reaction, where positive reactions turned
316 yellow and negative reactions remained pink when observed by the naked eye. To
317 further confirm the specific amplification of the target region, the gradient LAMP
318 products were visualized by DNA staining and gel electrophoresis for the amplified
319 product, further confirming the detection limit of LAMP (**Figure 2D**, lower panel).

320

321 **2.3. Specificity of the novel LAMP with other respiratory and medically** 322 **important viruses**

323 The SARS-CoV-2 embraces genetic and phenotypic features of several common cold
324 coronaviruses and other viruses of the respiratory tract. Owing to high genetic
325 similarity (up to 96% at nucleotide levels) and common respiratory specimen for
326 clinical identification of CoVID-19 patients, we aimed to investigate any non-specific
327 amplification in the LAMP assay. In order to demonstrate the specificity of the LAMP
328 assay, we used pathogens belonging to 5 families of the most important medical and
329 respiratory viruses. As shown in the **Figure 3A**, the qRT-PCR specifically detected
330 only the SARS-CoV-2 and this specificity was noticed on Gel-red staining of amplified
331 products (**Figure 3B**). Consistently, no cross-reactivities were noticed with the LAMP
332 in both colorimetric detection (**Figure 3C**, upper panel) or electrophoreses (**Figure 3C**,
333 lower panel). Collectively, a high level of specificity was observed in primers set using
334 either of the assays.

335

336 **2.4. Temporal investigations of the LAMP and its impact on the limit of detection**

337 One of the major advantages of LAMP is its robustness. In order to determine the time
338 optimal for sufficient amplification of targeted genes, *in vitro* transcribed RNA was used
339 as a template for 30 minutes and assessed after every 5 minutes post-start of the
340 reaction. The change in colour was monitored visually by the naked eye. As shown in
341 Table 1, under equivalent conditions similar results were obtained from 20-30 minutes
342 of amplification. Therefore, 30 min was selected as the optimal visual interpretation
343 time for the results.

344

345 While the change in colour, reflective of a positive reaction, could be detected as early
346 as 20 minutes post-start of the reaction at lower copy number, subjective variabilities
347 may result in erroneous interpretation, especially in colorimetric based diagnostic
348 assays. To propose an automated imaging, processing and interpretation of the LAMP
349 based results, we developed a user-friendly device and furnished it with an artificial
350 intelligence based automatic interpretation algorithm.

351

352 **2.5. Manufacture of an isothermal nucleic acid amplification device with** 353 **colorimetric detection features**

354 A device (**Figure 4A**) was built with many off-the-shelf electronic components and
355 custom flexible resistive heating elements (5W, NEL, UK), and specially designed
356 aluminium heating blocks. Raspberry Pi (RPI) was used to control the device. The one
357 wire interface of the RPi was used to connect ten digital temperature sensors
358 (DS18B20, Maxim Integrated, USA) positioned directly on the PCB boards to monitor
359 heater block temperature changes and provide feedback control. The specially
360 designed aluminium heater blocks to hold 200 μ l PCR tubes and the lid heater to
361 prevent condensation were attached directly on top of the surface mount temperature
362 sensors on the respective PCBs with a heat transferring adhesive (TermoGlue,
363 Termopasty Grzegorz Gasowski, Poland). The flexible resistive heating elements
364 were also attached to the heater blocks. To circumvent the need for specialised docks
365 and eliminate user interpretation of the colorimetric results, a Raspberry Pi Camera
366 (RPi Camera) was used. Eight LEDs (LW T733, Osram, Germany) were assembled
367 on the top side of the lid mount PCB to shine light directly into the reaction tubes to
368 achieve consistent lighting within the device. All the above components were
369 assembled into a 3D printed enclosure (14.3 x 10.8 x 6 cm) specially designed with
370 openings to access to the USB and TCP/IP ports of the RPi. A 20,000 mAh power
371 bank (Anker Power Core, Anker, China) with two 5V, 2A output was used to power the
372 device. A Python based control software was used to control the heating, image the
373 progression of the LAMP assay and store the 'time-lapse' images and temperature
374 data within a specified folder. The user can initiate a test by either connecting to a
375 screen via the HDMI port or through simply pairing the device with the mobile app via
376 Bluetooth and selecting the required diagnostic assay.

377

378 **2.6. Automated image acquisition and processing through template matching-** 379 **based algorithm**

380 The LAMP assay in 8 separate tubes was remotely started to initiate heating to 65°C.
381 Images of those test tubes were captured using the inbuilt RPi Camera for every 20
382 seconds and were saved in the RPi in the RGB format. Each individual image
383 consisted of 8 frames around each tube with a black background. As the tube area
384 exposing colour changes was fractionally small compared to its background, we first
385 extracted each targeted tube frame from the image before applying an image
386 processing algorithm. In order to process these extracted frames, a reference tube
387 was selected as a template, and a template matching algorithm [21] was applied to
388 extract all tubes from the first image. The rationale for the template matching was to
389 search and find the location of a template image in a larger image. It simply slides the
390 template image over the input image to perform the 2-dimensional convolution and
391 compared values to get the maximum overlap to decide the exact similar areas.
392 Assuming that positions of the test-tube do not change over the time of an experiment,
393 images were cropped in an experiment to obtain the tube frames from the entire
394 image. These crops are then saved into a 2-dimensional array for RGB colour space

395 (see equation below). Once extracted, RGB format images were converted to YUV
396 format using the following transformation [22] to avoid diffraction and lighting
397 variabilities in different images.
398

$$399 \quad \begin{pmatrix} Y \\ U \\ V \end{pmatrix} = \begin{pmatrix} +0.257 & +0.504 & +0.098 \\ -0.148 & -0.291 & +0.439 \\ +0.439 & -0.368 & -0.071 \end{pmatrix} \cdot \begin{pmatrix} R \\ G \\ B \end{pmatrix} + \begin{pmatrix} 16 \\ 128 \\ 128 \end{pmatrix}$$

400
401 In YUV colour space, the Y channel represented the luminance of the colour, while
402 the U and V channels represented the chrominance (**Figure 4B**). Separating the
403 luminance from the chrominance reduced the effect of light changing and shadow
404 noises in each tested tube [23]. Finally, the chrominance (U, V) channels from the
405 YUV image were considered for image processing. The chrominance (U, V) values of
406 those extracted test tubes were compared with reference orange test tubes in positive
407 control and reference pink image in negative control test tubes to calculate the sum of
408 absolute difference (SAD) for each of the pixel values. After experiments with two
409 images set and fine tuning the threshold values manually, a SAD threshold value was
410 achieved which provides 100% accuracy in the separation of classes.
411

412 Despite the SAD based approach resulting in 100% accuracy for the images after 30
413 minutes, this approach failed with other datasets containing bubbles and different
414 background lights as a different threshold value was produced for each image set.
415 Therefore, a deep learning-based approach was utilised in our experiments to
416 generalize the classification for different background light and sound sources.
417

418 **2.7. Artificial intelligence-assisted rapid detection of colour changes** 419 **associated with the LAMP reaction**

420 Multiple rule-based computer vision techniques were applied to identify small changes
421 in light intensity and to fix the position. Deep learning is a subdomain of AI which
422 doesn't require any domain knowledge to work, however, it learns hidden patterns
423 from examples present in the dataset. A deep learning Convolutional Neural Network
424 (CNN) [24] architecture was proposed with the bespoke 8 layers deep mode as shown
425 in **Figure 4C**. It consisted of four convolutional layers followed by 2 dense and an
426 output layer. To compile the model, binary cross-entropy was used as a loss of
427 function and used to optimize.
428

429 For the training of the network, the dataset was shuffled and then split into 9:1
430 proportion (**Figure 4D**). 90% of the data was used to train the network and the
431 remaining 10% was exploited to check how the network behaved on seeing a new
432 image. Training a dataset requires loading numerous images into the memory in a
433 single operation which is an expensive process. Therefore, a data generator was
434 implemented that read the data in batches from the dataset directory and fed it to the
435 model. After multiple experiments, it was observed that the network converged after 6
436 cycles (epochs) through the dataset. Therefore, we ran an experiment for only 6
437 epochs to decrease the probability of overfitting. In addition, an additional set of 108
438 test-tube crops was used to validate the network. The best performing network
439 resulted in an accuracy of 98% in classifying tubes based on their colours (images
440 with better light).
441

442 In order to assess the temporal impact of the AI-assisted detection of colour changes
443 (indicative of amplification), the RT-LAMP reaction was run with 3 previously
444 confirmed positive and negative patient samples as well as positive and negative
445 controls. Colour changes were assessed every 5 minutes until the complete stoppage
446 of the LAMP reaction at 30 minutes. Gradual colour changes were detectable with the
447 naked eye as early as 20 minutes post-start of the reaction (**Figure 5A**).
448 Corresponding samples were run on the newly developed device and temporal and
449 real-time colour changes were monitored as described earlier. Depending upon the
450 viral load in the sample, a clear colour change was calibrated as early as 20 minutes
451 using device operated processing of the data (**Figure 5B**). Once the positive test
452 control is identified as positive, the test will be stopped, and results will be returned to
453 reduce the waiting time and power consumption on heating.

454
455 As shown in Fig 5B, template matching algorithm is applied to extract test tubes and
456 CNN model is applied and trained. The CNN model is used as machine learning
457 algorithm to identify colours for each image taken throughout the experiment. Images
458 taken at time tare marked as 't' in the Fig 5B. Once positive control test and negative
459 control test give the correct results consecutively for three times, LAMP based test will
460 be stopped, and results will be returned. This approach will reduce the waiting time for
461 the results and power consumption due to heating in the experiment.

462 **2.8. Validation of ai-LAMP and comparative performance in clinical settings**

463 In order to assess the field application of the optimized assay, we applied the ai-LAMP
464 to purified RNA spiked with miR-cel-miR-39-3p from CoVID-19 patients. A total of 199
465 swab samples were collected from CoVID-19 clinically suspected patients during
466 routine screening at the Royal Lancaster Infirmary (RLI), University Hospitals of
467 Morecambe Bay NHS Foundation Trust UK. The extracted RNA from swab samples
468 were run in parallel for ai-LAMP and two WHO/PHE recommended qRT-PCR targeting
469 the RdRP and N genes of the SARS-CoV-2. This parallel assessment allowed us to
470 assess the comparative performance of the ai-LAMP.

471
472 The RdRP gene-based qRT-PCR detected a total of 67 positives and 132 negatives
473 in a cohort of 199 patients (**Figure 6A**). In contrast, a higher number of positive (n=88)
474 and lower numbers of negative (n=111) were detected by the qPCR which targeted
475 the N gene (**Figure 6B**). Interestingly, the ai-LAMP detected a total of 126 positive
476 samples which constituted several times higher than RdRP and N gene-based qPCR,
477 respectively. Comparative analysis of these three molecular detection assays
478 revealed 58 total true positives (TP), 09 false negatives (FN), 64 true negatives (TN),
479 and 68 false positives (FP) in RdRP-based qRT-PCR compared to RdRP-based
480 LAMP (**Figure 6A**). Similarly, upon comparative analysis of the N gene-based qPCR
481 and RdRP-based LAMP, we observed a total of 74 TP, 14 FN, 59 TN, and 52 FP
482 (**Figure 6B**).

483
484 In the current clinical settings, a qRT_PCR targeting two genes (N and RdRP) was
485 conducted to conclusively identify CoVID-19 positive cases and this assay is referred
486 as cumulative (CUM) qRT-PCR. In this scenario, a sample would be considered as
487 positive only if a Ct value of ≥ 35 was detected in both N and RdRP-gene based
488 qRT-PCR. Using this approach, we noticed a total of a 70 positive and 129 negative
489 samples and an improved true positive (n=61), false negatives (n=09), true negatives
490 (n=64), and false positives (n=65) limits (**Figure 6C**). Taken together, the cumulative
491

492 comparative picture of the qPCR and ai-LAMP has identified a superior detection of
493 positive cases (**Figure 6D**). In order to confirm this detection performance, all ai-LAMP
494 amplification products were visualised by electrophoresis (data not shown), further
495 confirming the aided-detection and improved implication of ai-LAMP in the field
496 condition.

497
498 We next determined the detection limit of the ai-LAMP in direct correlation with the
499 standard Ct values of the qPCRs. Plotting of ai-LAMP positive and negative data
500 against the linearity of the Ct values revealed that ai-LAMP carried Cp (cycle number
501 at detection threshold) of up to 37 Ct determined in the qPCR based on the RdRP
502 gene (**Figure 6E and Supplementary Table 1**) or N gene (**Figure 6F and
503 Supplementary Table 1**) of the SARS-CoV-2. This detection is approximately 2 Ct
504 values higher than the detection limit of the standard qPCR. Analysis of the first 96
505 samples, run in parallel for the ai-LAMP, (**Figure 6G and Supplementary Table 1**)
506 showed a clear demarcation of the positive and negative samples in the RdRP-gene
507 based ai-LAMP. In order to rule out the quantitative recovery from spiked miRNA, a
508 qRT-PCR was run for 40 randomly selected samples [37]. Based on the Ct values, all
509 samples showed a marked recovery except a single sample where a low detection of
510 the miRNA was identified (**Figure 6H, Supplementary Table 1 and Supplementary
511 Figure 1**).

512
513 Collectively, these data highlight the improved specificity and sensitivity of the AI-
514 assisted LAMP assay compared to the naked-eye interpretation of the LAMP-
515 positivity, thus enhancing the timely and automated detection and interpretation of the
516 assay results.

517

518 **3. Discussion**

519

520 The SARS-CoV-2 is now a global pandemic, over 216 countries are currently reporting
521 active infections around the globe and the number of daily infections and deaths is
522 continuing to increase, especially in the Americas and South East Asia in a series of
523 multiphasic spread [25]. Currently, there is no licensed vaccine or registered drugs,
524 leaving timely identification of CoVID-19 patients, contact tracing and isolation of
525 positive contacts as the most effective means of containing the pandemic. Among
526 different molecular diagnostic chemistries, the LAMP technology provides a promising
527 approach for rapid and reliable detection in resource-limited settings [14]. Recently,
528 the LAMP technology has been widely applied for the identification of West Nile virus,
529 influenza virus, yellow fever virus, Marburg virus, Ebola virus, Zika virus, and other
530 myriads of viruses [26- 31].

531

532 The genome of SARS-CoV-2 is approximately 30kb in size with a coding capacity of
533 9860 amino acids. All of the β -coronaviruses encodes for structural (replicases, S, E,
534 M and N) genes in the order of 5' to 3' in the positive sense genome [5, 32, 33]. A
535 range of qRT-PCRs have been proposed and are referred by the World Health
536 Organization [25; [https://www.who.int/emergencies/diseases/novel-coronavirus-
537 2019/technical-guidance/laboratory-guidance](https://www.who.int/emergencies/diseases/novel-coronavirus-2019/technical-guidance/laboratory-guidance)] for diagnosis of SARS-CoV-2. While
538 diagnostic assays can be designed on the most conserved region of the viral genome,
539 most of the routinely applied RT-PCR and RT-LAMP have been targeting the S, N,
540 RdRP, and ORF1a/b genes mainly due to their high level of transcription and
541 abundance in expression compared to other genes of the SARS-CoV-2 [5, 6]. For the

542 detection of SARS-CoV-2, Chan et al., [34] have targeted and developed a standard
543 RT-LAMP with LoD of 11.2 RNA copies/reaction using *in vitro* RNA transcripts. Yan et
544 al., [13] have adapted the ORF1ab to developed RT-LAMP assay with a detection limit
545 of sensitivities of 2×10^1 copies per reaction. The majority of these diagnostic assays
546 carry a high level of sensitivity, specificity and repeatability; however, these primarily
547 lack the clinical validation and/or optimization on the synthetic targets.

548
549 In this study, we have developed and evaluated a novel RT-LAMP in one of the most
550 conserved genes (i.e. RdRP) within the SARS-CoV-2 genome. The RT-LAMP was
551 then directly compared with the currently applied routine diagnostic assays to assess
552 the comparative performance. The RT-LAMP assay developed in this study, could
553 detect as low as 100 copies with an *in vitro* RNA transcript. Importantly, the RT-LAMP
554 has detected the SARS-CoV-2 RNA in 68/199 (34%) and 52/199 (26%) additional
555 specimens that were tested negative by the RdRP-based qRT-PCR and N-based
556 qRT-PCR, respectively. These findings are interesting, both clinically and
557 epidemiologically due to the high proportion of asymptomatic and mildly symptomatic
558 cases of CoVID-19. These apparently healthy people have been suggested as major
559 sources of virus propagation and basis of epidemics within the community [34, 35, 36].
560 Due to the large number of cases (~5000) in the testing facility, additional positive
561 specimens could have been detected by the RT-LAMP which might have remained
562 undetected by the qRT-PCRs. Using of an internal standard that is not expressed in
563 humans such as cel-miR-39-3p can alleviate the problem of an effective RNA
564 extraction approach. In addition, we used a fixed total RNA concentration in all
565 experiments allowing for better comparisons across groups.

566
567 The main challenges of using the Colorimetric approach are background which
568 changes the colour perspective, issues in identifying small changes, bubbles in the
569 test tubes, relatively small area corresponding to colour change and pixel variation
570 due to camera flash and background reflections. The CNN based model has used
571 high-performance computer images to train using these issues and having learned the
572 patterns is able to classify colour, despite the presence of noise. The trained model
573 has successfully moved to Rpi to identify colour changes in test tubes. The study
574 produced 98% accuracy for images taken with better light (Open) and the duration of
575 testing could be dynamically controlled to reduce the length of operating time and
576 heating with a resulting reduction in energy consumption by the device.

577
578 Collectively, our data showed that the newly established ai-LAMP was highly specific
579 for the detection of SARS-CoV-2 RNA *in vitro* and in respiratory tract clinical
580 specimens. The usage of this novel LAMP assay might be helpful especially for
581 detecting COVID-19 cases with low viral loads and when testing upper respiratory tract
582 specimens from patients. Development of ai-LAMP into a multiplex assay which can
583 simultaneously detect other human-pathogenic coronaviruses and respiratory
584 pathogens may further increase its clinical utility in the future.

585 586 **Acknowledgements**

587 The authors would like to thank the Electronic Technicians William Schkzhamian,
588 Gopalakirishnan Jeysundra and Michael Lateo of Brunel University London for their
589 efforts to come into the University with special permission during the early lockdown
590 period to produce eight laboratory prototypes within 5 days. We thank the Microbiology
591 Department, University Hospitals of Morecambe Bay for access to anonymised patient

592 samples and acknowledge the support of BLS Lancaster University Technicians
593 throughout the lockdown period. We would like to thank Dr Derek Gatherer, Lancaster
594 University, in aligning large SARS-COV-2 genome sequences.

596 **Disclosure statement**

597 No potential conflict of interest was reported by the authors.

598

599 **Funding**

600 The authors wish to express our sincere appreciation to the BBSRC for allowing us to
601 repurpose the LAMP prototypes produced in the grant BB/R012695/1 to be used for
602 SARS-CoV-2 laboratory testing at The University of Lancaster. We would like to thank
603 the support of BBSRC (BB/M008681/1 and BBS/E/I/00001852) and British Council
604 (172710323 and 332228521) at Division of Biomedical and Life Sciences, Lancaster
605 University, UK. We would also like to thank Brunel University London and the
606 University of Surrey for providing some financial support to rapidly produce these
607 devices.

608

609 **References**

610

611 [1] Zhu N, Zhang D, Wang W, et al. A novel coronavirus from patients with pneumonia
612 in China, 2019. *N Engl J Med*. 2020 Feb 20;382(8):727-733.

613 [2] Chan JF, Yuan S, Kok KH, et al. A familial cluster of pneumonia associated with
614 the 2019 novel coronavirus indicating person-to-person transmission: a study of a
615 family cluster. *Lancet*. 2020a;395:514–523.

616 [3] Zhou P, Yang XL, Wang XG, et al. A pneumonia outbreak associated with a new
617 coronavirus of probable bat origin. *Nature*. 2020 Mar;579(7798):270-273.

618 [4] Decaro N and Lorusso A. Novel human coronavirus (SARS-CoV-2): A lesson from
619 animal coronaviruses. *Vet Microbiol*. 2020 May;244:108693.

620 [5] Chan JF, Kok KH, Zhu Z, et al. Genomic characterization of the 2019 novel human-
621 pathogenic coronavirus isolated from a patient with atypical pneumonia after visiting
622 Wuhan. *Emerg Microbes Infect*. 2020; 9(1): 221–236.

623 [6] Kim D, Lee J, Yang J, et al. The Architecture of SARS-CoV-2 Transcriptome. *Cell*.
624 2020 May 14;181(4):914-921.e10.

625 [7] Peiris JS, Lai ST, Poon LL, et al. Coronavirus as a possible cause of severe acute
626 respiratory syndrome. *Lancet*. 2003 Apr 19;361(9366):1319-25.

627 [8] Woo PC and Yuen KY. Severe acute respiratory syndrome coronavirus as an agent
628 of emerging and reemerging infection. *Clin Microbiol Rev*. 2007 Oct; 20(4): 660–694.

629 [9] Yuen KY. Middle East respiratory syndrome coronavirus: another zoonotic
630 betacoronavirus causing SARS-like disease. *Clin Microbiol Rev*. 2015 Apr;28(2):465-
631 522.

632 [10] WHO, Novel Coronavirus – China 2020a. [https://www.who.int/csr/don/12-january-
633 2020-novel-coronavirus-china/en/](https://www.who.int/csr/don/12-january-2020-novel-coronavirus-china/en/)

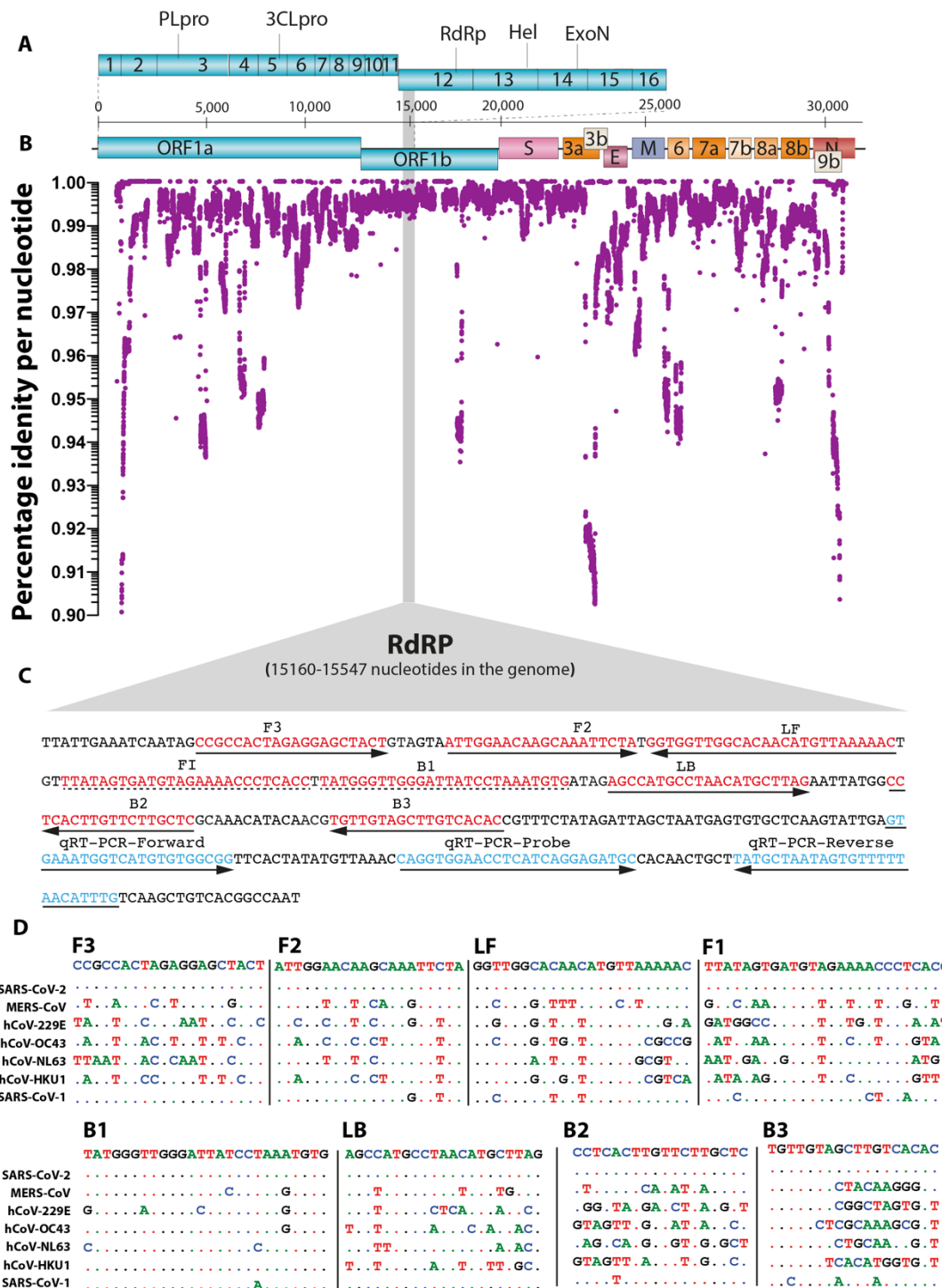
634 [11] Vogels CBF, Brito AF, Wyllie AL, et al. Analytical sensitivity and efficiency
635 comparisons of SARS-COV-2 qRT-PCR assays. medRxiv.
636 2020;2020.03.30.20048108. Available
637 from: <https://medrxiv.org/content/early/2020/04/01/2020.03.30.20048108>.

638 [12] Kashir J and Yaqinuddin A. Loop mediated isothermal amplification (LAMP)
639 assays as a rapid diagnostic for COVID-19. *Medical Hypotheses*. 2020;141.
640 doi:10.1016/j.mehy.2020.109786.

- 641 [13] Yan C, Cui J, Huang L, et al. Rapid and visual detection of 2019 novel coronavirus
642 (SARS-CoV-2) by a reverse transcription loop-mediated isothermal amplification
643 assay. *Clin Microbiol Infect.* 2020 June; 26(6):773-779.
- 644 [14] Mori Y and Notomi T. Loop-mediated isothermal amplification (LAMP): Expansion
645 of its practical application as a tool to achieve universal health coverage. *J Infect*
646 *Chemother.* 2020 Jan;26(1):13-17.
- 647 [15] Mahony J, Chong S, Bulir D, et al. Development of a sensitive loop-mediated
648 isothermal amplification assay that provides specimen-to-result diagnosis of
649 respiratory syncytial virus infection in 30 minutes. *J Clin Microbiol.* 2013
650 Aug;51(8):2696-701.
- 651 [16] Ganguli A, Ornob A, Yu H, et al. Hands-free smartphone-based diagnostics for
652 simultaneous detection of Zika, Chikungunya, and Dengue at point-of-care. *Biomed*
653 *Microdevices.* 2017 Aug 22;19(4):73.
- 654 [17] Kaarj K, Akarapipad P, Yoon JY. Simpler, Faster, and Sensitive Zika Virus Assay
655 Using Smartphone Detection of Loop-mediated Isothermal Amplification on Paper
656 Microfluidic Chips. *Sci Rep.* 2018 Aug 18;8(1):1-11.
- 657 [18] Yu L, Wu S, Hao X, et al. Rapid colorimetric detection of COVID-19 coronavirus
658 using a reverse transcriptional loop-mediated isothermal amplification (RT-LAMP)
659 diagnostic platform: iLACO. *Clin Chem.* 2020; 0:0,1–3, doi:10.1093/clinchem/hvaa102
- 660 [19] Nguyen T, Bang DD, Wolff A. 2019 Novel coronavirus disease (COVID-19):
661 Paving the road for rapid detection and point-of-care diagnostics. *Micromachines*
662 (Basel). 2020 March;11(3):306.
- 663 [20] Katoh K, Rozewicki J, Yamada KD. MAFFT Online Service: Multiple Sequence
664 Alignment, Interactive Sequence Choice and Visualization. *Brief Bioinform.* 2019 Jul
665 19;20(4):1160-1166.
- 666 [21] Sun Y, Mao X, Hong S, et al. Template Matching-Based Method for Intelligent
667 Invoice Information Identification. *IEEE Access.* 27 February 2019;7:28392-28401.
- 668 [22] Yang G, Li H, Zhang L, et al. Research on a skin color detection algorithm based
669 on selfadaptive skin color model; 2010 International Conference on Communications
670 and Intelligence Information Security, Nanning, China. *IEEE Xplore.* 2010; 266-270.
- 671 [23] Al-Tairi, ZH, Rahmat RWO, Saripan MI, et al. Skin Segmentation Using YUV and
672 RGB Color Spaces. *J Inf Process Syst.* 2014 June;(10)2: 283-299.
- 673 [24] Sharif M, Khan MA, Rashid M, et al. Deep CNN and geometric features-based
674 gastrointestinal tract diseases detection and classification from wireless capsule
675 endoscopy images. *J Ex Theor Artif In.* 01 Feb 2019 Feb,
676 doi.org/10.1080/0952813X.2019.1572657
- 677 [25] WHO, Coronavirus disease (COVID-19) pandemic 2020b.
678 <https://www.who.int/emergencies/diseases/novel-coronavirus-2019>
- 679 [26] Kurosaki Y, Grolla A, Fukuma A, et al. Development and evaluation of a simple
680 assay for Marburg virus detection using a reverse transcription-loop-mediated
681 isothermal amplification method. *J. Clin. Microbiol.* 2010 April 26; 48:2330–2336.
- 682 [27] Ge Y, Wu B, Qi X, et al. Rapid and sensitive detection of novel avian-origin
683 influenza A (H7N9) virus by reverse transcription loop-mediated isothermal
684 amplification combined with a lateral-flow device. *PLoS One.* 2013 Aug
685 1;8(8):e69941.
- 686 [28] Kwallah A, Inoue S, Muigai AW, et al. A real-time reverse transcription loop-
687 mediated isothermal amplification assay for the rapid detection of yellow fever virus.
688 *J. Virol. Methods.* 2013 Oct;193(1):23-7.

689 [29] Cao Z, Wang H, Wang L, et al. Visual detection of west nile virus using reverse
690 transcription loop-mediated isothermal amplification combined with a vertical flow
691 visualization strip. *Front. Microbiol.* 2016 Apr 20;7:554.
692 [30] Xu C, Wang H, Jin H, et al. Visual detection of Ebola virus using reverse
693 transcription loop-mediated isothermal amplification combined with nucleic acid strip
694 detection. *Arch. Virol.* 2016 May;161(5):1125-33.
695 [31] Chotiwan N, Brewster CD, Magalhaes T, et al. Rapid and specific detection of
696 Asian- and African- lineage Zika viruses. *Sci. Transl. Med.* 2017 May
697 3;9(388):eaag0538.
698 [32] Chen L, Liu W, Zhang Q, et al. RNA based mNGS approach identifies a novel
699 human coronavirus from two individual pneumonia cases in 2019 Wuhan outbreak.
700 *Emerg Microbes Infect.* 2020; 9(1): 313–319.
701 [33] Lu R, Zhao X, Li J, et al. Genomic characterisation and epidemiology of 2019
702 novel coronavirus: implications for virus origins and receptor binding. *The Lancet.*
703 2020 February 22;395:565–574.
704 [34] Chan JF, Yip CC, To KK, et al. Improved molecular diagnosis of COVID-19 by the
705 novel, highly sensitive and specific COVID-19-RdRp/Hel real-time reverse
706 transcription-PCR assay validated in vitro and with clinical specimens. *J Clin*
707 *Microbiol.* 2020 Apr 23;58(5):e00310-20.
708 [35] Wei M, Yuan J, Liu Y, et al. Novel coronavirus infection in hospitalized infants
709 under 1 year of age in China. *JAMA.* 2020;323(13):1313-1314.
710 [36] Shahid, M, Amin, I, Afzal, S, Fatima Z, Idrees, M. Comparative Analysis of
711 Immunological and Genomic Outcomes of Dengue Virus Outbreak in Pakistan.
712 *Pakistan J. Zool.*, Vol. 51, Iss. 5, pp 1971-1974
713 [37] Sodi, R, Eastwood, J, Caslake, M, et al. Relationship Between Circulating
714 microRNA-30c With Total- And LDL-cholesterol, Their Circulatory Transportation and
715 Effect of Statins. *Clin Chim Acta.* 2017 Mar;466:13-19
716
717
718
719
720
721
722
723
724
725
726
727
728
729
730
731
732
733
734
735
736
737
738

739



740

741

742

743

744

745

746

747

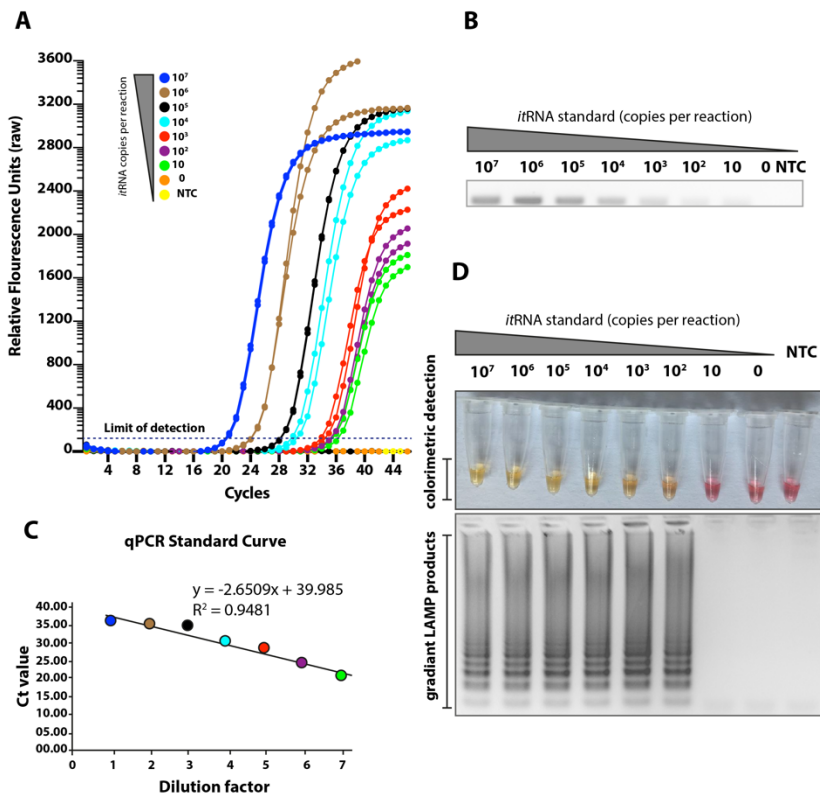
748

749

750

Figure 1: In silico analysis of SARS-CoV-2 and primer design. (A) Genome organization of SARS-CoV-2. Scale represents an approximate position of the genome whereas ORF1a and b are expanded to show internal gene organization. **(B)** Level of gene identity across the genome of the SARS-CoV-2. Identity less than 90% is not shown. **(C)** Primer location in the RdRp gene of SARS-CoV-2 is shown. Red coloured sequences represent LAMP primers whereas blue coloured sequences are primers and probes used in the qRT-PCR. **(D)** Comparative sequence identity using the primers against different human coronaviruses compared to the reference SARS-CoV-2 sequence; dots represent identical nucleotides.

751



752

753

754 **Figure 2: Sensitivities of the LAMP assay.** (A) Seven different dilutions of in vitro
 755 transcribed RNA were run for quantitatively measurement in the qRT-PCR. Relative
 756 fluorescence units show a gradient decrease in signals. (B) The corresponding PCR
 757 products on the electrophoresis gel (C) The qRT-PCR standard curve based on the
 758 Ct value and dilution factor. (D) The serially diluted synthetic RNAs were run for LAMP
 759 assay and colour change represents positive (yellow) or negative (pink). The lower
 760 panel show LAMP gradient products.

761

762

763

764

765

766

767

768

769

770

771

772

773

774

775

776

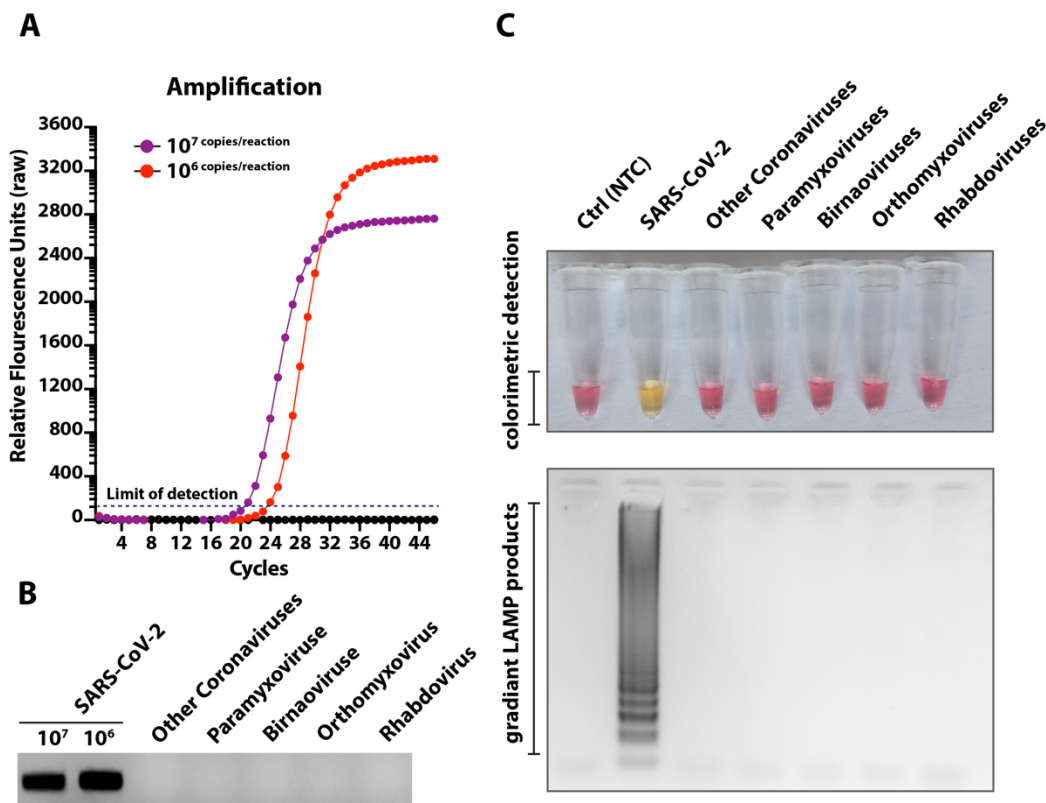
777

778

779

780

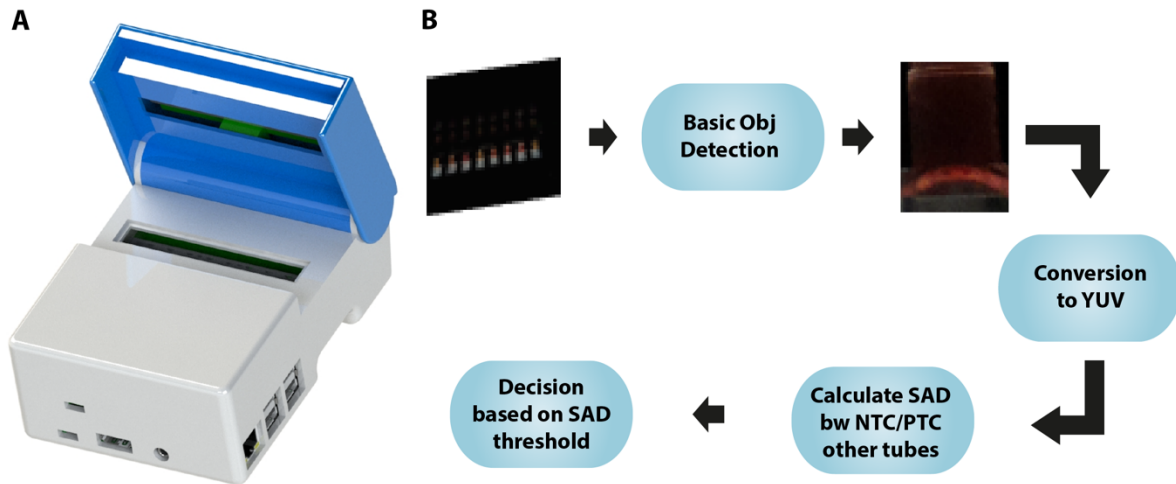
781
782



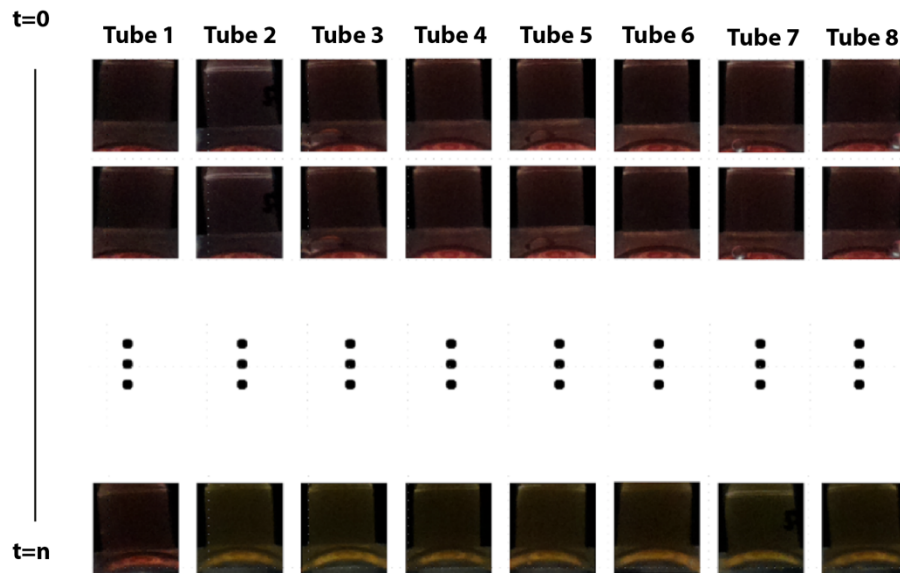
783
784
785
786
787
788
789
790
791
792
793
794
795
796
797
798
799
800
801
802
803
804
805
806
807
808
809

Figure 3: Specificity of the LAMP assay. (A) RNA extracted from different medically or respiratory important viruses as well as two dilutions of synthetic RNA were run for qPCR. (B) Corresponding PCR products were run on gel to demonstrate specificity. (C) Similar to qRT-PCR, extracted RNA were run for the LAMP assay. The top panel indicates the colorimetric detection of LAMP positive/negative reactions and the lower panel show the electrophoresis of the corresponding LAMP products.

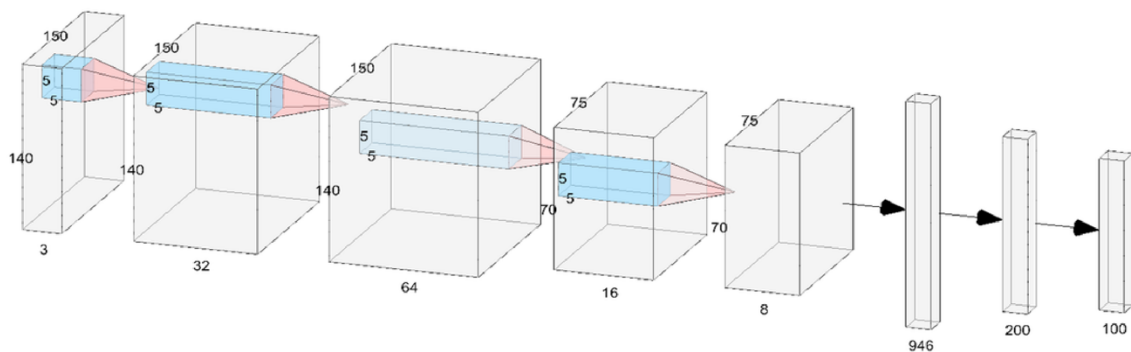
810



C



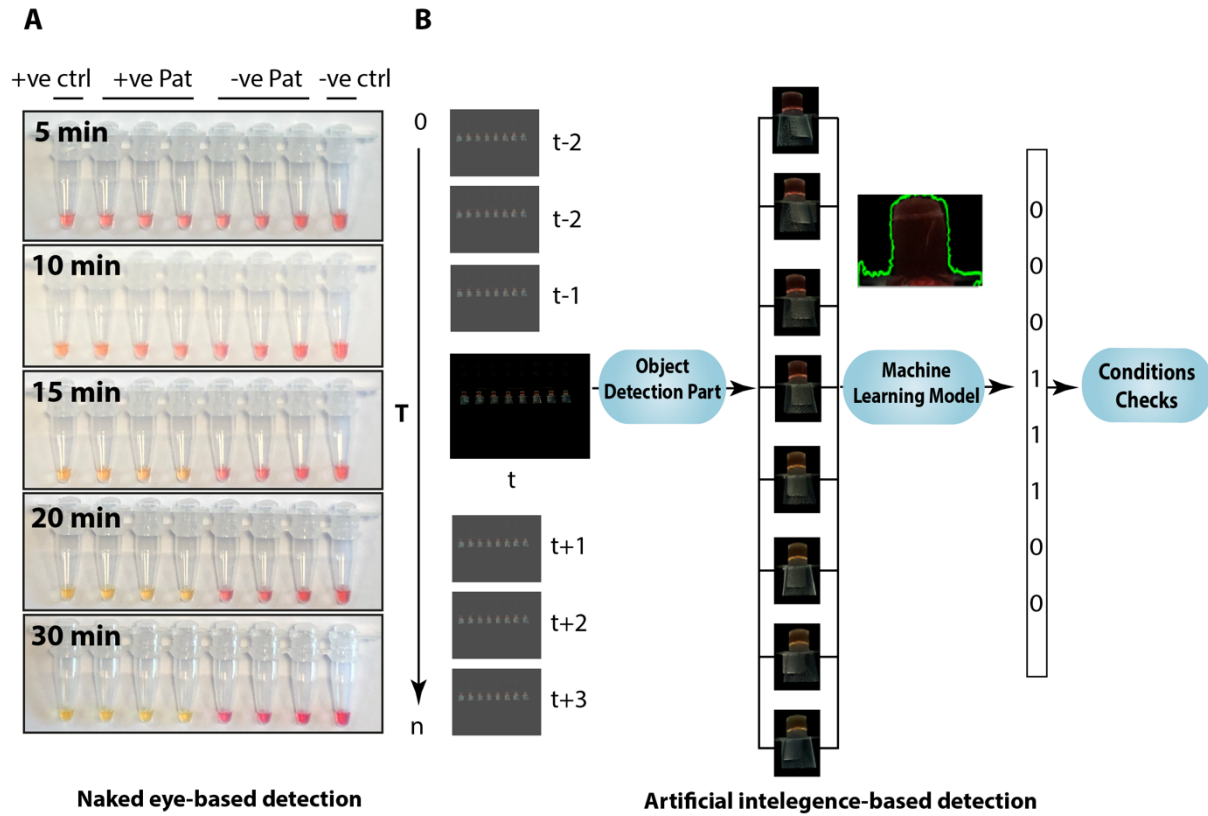
D



811
812
813
814
815
816
817

Figure 4: Fabrication and processing of LAMP data for enhanced detection of SARS-CoV-2. (A) Exterior of a smart diagnostic device **(B)** Description of the AI-assisted algorithm and image processing. **(C)** Pipeline to process images and extraction of colorimetric information. **(D)** Schematic outlining the training of the network for image processing.

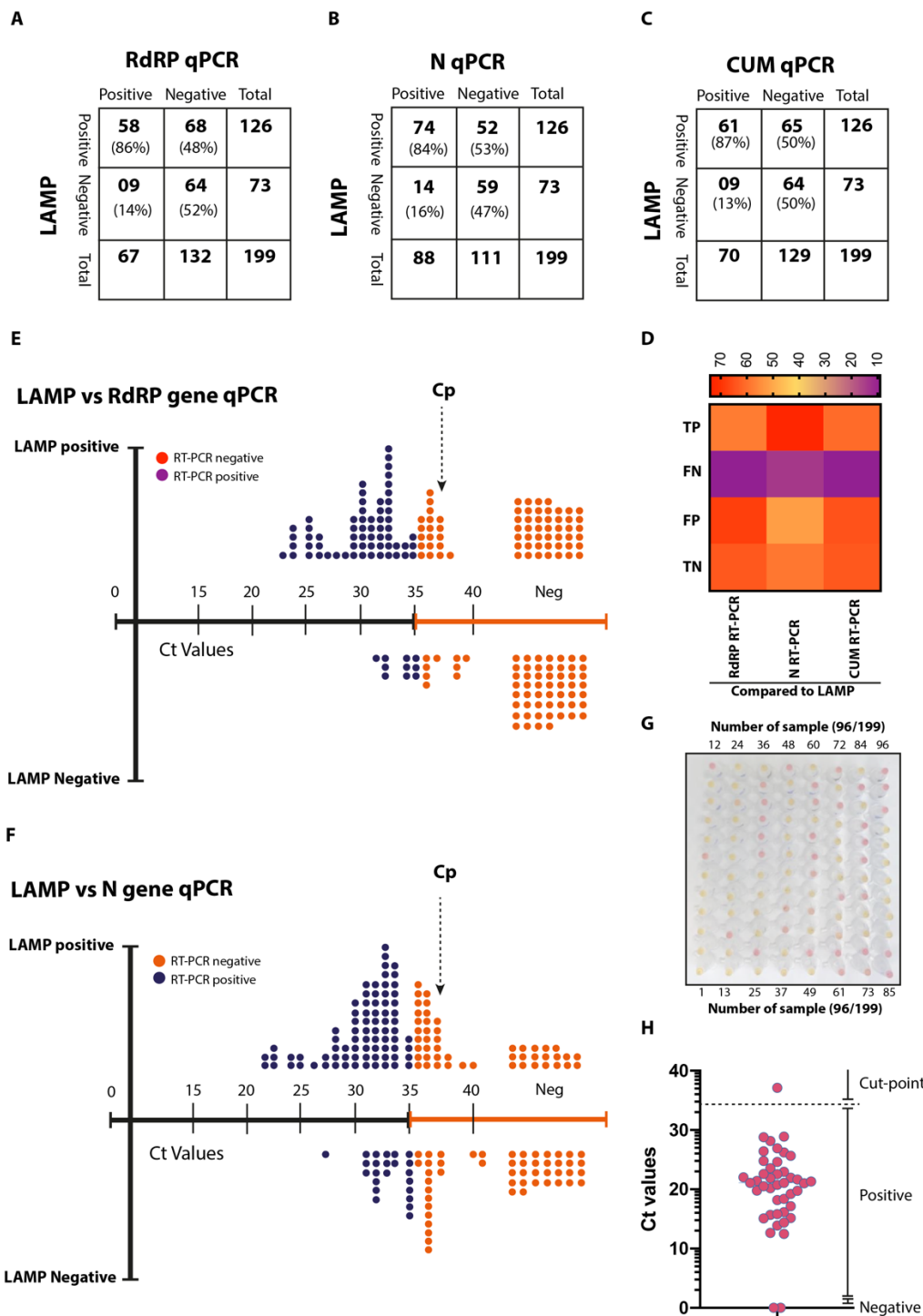
818



819
820
821
822
823
824
825

Naked eye-based detection **Artificial intelligence-based detection**

Figure 5: Conventional and AI-assisted interpretation of LAMP results. (A) Temporal analysis of known positive and negative patient samples for visual interpretation of LAMP results. **(B)** Interpretation of corresponding patient samples by the AI-assisted LAMP results.



826
827
828
829
830
831
832
833
834
835
836
837

Figure 6: Clinical validation of ai-LAMP. (A-C) Comparative sample positivity between LAMP and RdRP qRT-PCR (A), LAMP and N qRT-PCR (B), LAMP and CUM qRT-PCR results (C). (D) The heatmap indicate the relative positive and negative samples among three assays. (E) Linearity chart comparing the LAMP positive/negative samples and their detection based on the RdRP gene-based qRT-PCR. (F) Linearity chart comparing the LAMP positive/negative samples and their detection based on the N gene-based qRT-PCR. (G) Naked eye detection of first 96 samples out of the total 199 patients' samples processed. (H) Recovery Ct values of the miRNA from spiked before RNA extraction.